IEEE Access
Multidisciplinary ⋮ Rapid Review ⋮ Open Access Journal

Received 29 July 2024, accepted 24 August 2024, date of publication 27 August 2024, date of current version 5 August 2025.

Digital Object Identifier 10.1109/ACCESS.2024.3450611

RESEARCH ARTICLE

Seamless Integration of Grid-Forming and Grid-Following Capabilities in a Single VSI Within a Unified Hybrid Control Framework Under Islanded Conditions

IMAN LORZADEH[1], (Member, IEEE), OMID LORZADEH[2], (Student Member, IEEE), DIMITAR V. BOZALAKOV[1,3], (Senior Member, IEEE), LUC DUPRÉ[1], (Member, IEEE), AND LIEVEN VANDEVELDE[1,3], (Senior Member, IEEE)

[1]Department of Electromechanical, Systems and Metal Engineering, Ghent University, 9052 Ghent, Belgium
[2]Senior Electrical Engineer – Power Electronics and Control, Natron Energy, San Francisco, CA 94568, USA
[3]FlandersMake@UGent—MIRO Core Laboratory, 9052 Flanders Make, Belgium

Corresponding author: Iman Lorzadeh (iman.lorzadeh@ugent.be)

ABSTRACT To achieve seamless integration of grid-forming (GFM) and grid-following (GFL) capabilities in a single voltage-source inverter (VSI) under islanded conditions, this study introduces a unified hybrid control (UHC) scheme with minimal control parameters and measurement sensors. The UHC scheme enables a single voltage-controlled VSI to emulate the behavior of two virtual parallel VSIs, each operating independently as a GFM and GFL inverter, thereby ensuring voltage and frequency stability, as well as reliable power sharing. The proposed UHC approach is designed specifically for islanded microgrids, providing functionalities for voltage-controlled inverters to perform multiple operational tasks simultaneously. These include voltage and frequency regulation, provision of local grid support services, and tracking of reference powers using output current control. The implementation utilizes a dual-loop parallel control strategy based on a proportional-resonant (PR) controller in the $\alpha\beta$ reference frame, which operates without requiring a phase-locked loop (PLL) in the islanded operational context. The control structure requires tuning of only three control parameters (two PR controller parameters and one active damping term), while the other parameters represent physical system values. Under the tested islanded operating conditions, VSIs equipped with the UHC scheme demonstrate the ability to mimic virtual inertia, contributing to voltage and frequency stability during sudden load changes, reference power variations, line outages, and short-circuit fault scenarios with appropriate dynamic and transient responses, addressing the specific challenges of islanded microgrid stability and control. Comprehensive simulation studies on single- and multi-inverter systems operating in the islanded mode validate the effectiveness and feasibility of the UHC scheme for practical implementation in power systems.

INDEX TERMS Grid-forming, grid-following, unified hybrid control, inverter-based resources, islanded operation mode.

I. INTRODUCTION

Traditional power grids rely on synchronous generators (SGs) to function as both grid-forming (GFM) and grid-following (GFL) resources. Within these grids, swing/slack buses, which acts as GFM sources, are pivotal in maintaining the grid frequency and voltage for stability. In contrast, GFL sources generate active and reactive power based on dispatch schedules or operator commands. The integration of renewable energy sources (RESs) and energy storage systems (ESSs) into AC grids through voltage source inverters (VSIs) has the potential to revolutionize large-scale centralized

The associate editor coordinating the review of this manuscript and approving it for publication was Nga Nguyen.

systems into power-electronics-based distributed systems. This structural transition has streamlined the coordination and integration of inverter-based resources (IBRs), elevating their significance in modern power systems over large centralized SGs [1], [2], [3]. The increasing adoption of inertia-less IBRs with grid-independent control poses a significant challenge to system reliability and stability compared with SG directly coupled to the grid, which offers mechanical inertia. This is because of the potential for instantaneous mismatches between the generation and demand. Interface inverters not only facilitate rapid responses to grid start-up but also provide a wide range of control strategies with desirable dynamic performance. This versatility is crucial for maintaining grid stability during transients, potentially obviating the necessity for protective measures, such as load shedding [4]. With IBRs now constituting over 65% of the generation in numerous global power grids and large grid subsystems, concerns regarding grid support, reliability, and stability have become increasingly pertinent [5]. These challenges become particularly critical in islanded microgrids, where the absence of a main grid connection necessitates robust control strategies for maintaining system stability and reliability without external support [3].

Interface inverters are classified as grid-following inverters (GFLIs) when operating in the grid-connected mode and grid-forming inverters (GFMIs) when operating in the islanded mode, based on their primary control strategy [2]. GFLIs function as current sources connected to an energized network, aligning the active and reactive power outputs with reference values. By contrast, GFMIs operate as voltage sources and establish and regulate the local grid voltage amplitude and frequency. Resource-associated inverters, which function as conventional GFLIs, are extensively utilized in RESs and ESSs to control output power based on specified reference values [6]. Despite their efficacy in power regulation, GFLIs cannot directly control the grid voltage and frequency or contribute to grid stability, as they maintain constant active and reactive power targets during transients. They rely heavily on external set-points for grid conditions, as monitored by an upstream supervisory system. This reliance results in delayed responses to changes in the grid parameters owing to communication latencies [5], [7]. This limitation persists unless adequate SGs or GFMIs are available to ensure a minimum level of inertia. This precautionary measure is crucial for preventing the initial rate of change of frequency (ROCOF) from threatening grid stability [5]. Conversely, GFMIs exhibit significantly faster responses than GFLIs in specific scenarios such as active power fast recovery and frequency support, particularly in islanded or weak grids. Consequently, GFMIs can mitigate frequency and voltage fluctuations to a risk-free rate of change, thereby contributing to grid stability. Moreover, the use of phase-locked loop (PLL)-based control in GFLIs may introduce challenges for maintaining grid voltage stability under specific grid disturbances or suboptimal tuning conditions [8], [9]. This challenge arises because of the positive feedback in the PLL control system, which can be readily substantiated through small-signal impedance models specifically tailored for voltage-instability analysis [9]. In islanded microgrids, these distinctions between GFLIs and GFMIs become particularly critical, as the absence of a stiff grid connection amplifies the impact of control strategy limitations on system stability and performance [10].

Research suggests that GFMIs offer superior grid support capabilities compared with GFLIs, even when additional control loops for synthetic inertia are implemented [10], [11]. Hence, as IBRs become more prevalent in future power grids, especially in isolated or off-grid scenarios, GFMIs are emerging as versatile and crucial alternatives. However, owing to the absence of a rotating mass, GFMIs require a sufficient energy buffer to provide a robust inertial response, mimicking the dynamic behavior of SGs and enhancing the grid frequency support during unexpected changes and contingencies [12], [13]. Therefore, the main operational limitations of GFMIs in islanded operation mode stem from their inability to precisely control output powers, which automatically vary with changing grid parameters, and the necessity for an energy buffer to ensure proper operation. To realize diverse applications in islanded conditions, there is a crucial need for an integrated control strategy that simultaneously leverages the advantages of GFMIs—grid voltage and frequency regulation and grid support capability (creating a stable reference grid)—and GFLIs, which precisely track reference powers (ensuring that power delivery matches demand accurately). Such a system could improve the reliability, efficiency, and stability of islanded power systems. Although a single GFMI can maintain grid stability under islanded conditions, it may struggle to handle rapid load changes with high precision in power delivery, potentially necessitating a larger energy buffer to manage fluctuations. Consequently, if a GFMI were capable of accurately tracking power references without delay, it could potentially match its output to the required power demand more effectively. This capability might reduce the immediate need for an energy buffer or lower the size and capacity requirements of the buffer by enabling the inverter to manage rapid power changes [13].

To achieve this, the parallel connection of a GFMI and GFLI, each with independent control structures, is considered the most straightforward approach [14]. However, this method entails increased installation costs, heightened hardware complexity, and a distinct control philosophy compared with a single-inverter system. Moreover, in this case, effective coordination between the control structures of the GFMI and GFLI is crucial to prevent conflicts and ensure smooth operation of the inverters. Another approach involves exploring the potential of a VSI that can flexibly transition between GFM and GFL modes based on the system conditions and demands. Accordingly, [15] introduced an integrated control scheme that combines GFM and GFL capabilities using Monte Carlo artificial bee colony-optimized fractional-order Proportional-Integral (PI) controllers to develop a single VSI. However, employing these optimization methods, coupled with scalability concerns, could add complexity to the design and implementation of control systems, especially in larger-scale power distribution systems. This added

complexity could increase the computational burden required for tuning and optimization. Moreover, developing a control strategy that can enable smooth mode transitions without introducing unstable transients remains a complex challenge. Therefore, in the context of islanded microgrids, there is a compelling research opportunity to develop a cost-effective hybrid control technique that can seamlessly integrate the advantages of GFMIs and GFLIs within a single voltage-controlled VSI, potentially enhancing system efficiency and reliability while minimizing the complexities associated with control switching, as initially explored in grid-connected systems by [20]. Unlike grid-connected applications, islanded systems present unique challenges due to the absence of a stiff grid reference, making the integration of these capabilities more critical for stability. This study addresses this research gap by examining how specialized control strategies can be developed to meet the unique requirements of islanded conditions.

A. RELATED WORKS AND LIMITATIONS OF EXISTING APPROACHES

Hybrid voltage and current control schemes have been applied in various key areas, including power quality [16], grid fault ride-through [17], and high-voltage direct current transmission systems [18]. A PLL-based hybrid control scheme was introduced in [19] that integrates GFM and GFL functionalities to achieve improved robustness and performance in IBRs. Nevertheless, one potential limitation of this control scheme is its susceptibility to noise and voltage stability challenges. While PLLs are designed for fast dynamic response, careful design is necessary to ensure robust operation under disturbance conditions, thereby maintaining voltage stability. In islanded microgrids specifically, PLL-based control methods face additional challenges due to the absence of a strong voltage reference, making the system more vulnerable to instabilities during disturbances and load changes [8].

The foundational concept of integrating GFM and GFL functionalities within a single inverter was initially introduced by Lima and Watanabe in [20]. Their hybrid control converter (HCC) employs a control architecture based on the *dq* reference frame, utilizing cascaded PI controllers with a PLL for grid synchronization. While their approach has demonstrated benefits in improving grid stability and consolidating inverter functionalities for grid-connected applications, several important limitations can be identified, particularly for islanded microgrid applications where the absence of a strong grid reference amplifies control challenges. It is worth noting that the HCC approach is derived from an equivalent circuit model that performs adequately under specific grid-connected conditions. However, the selection of control structures in power systems is not merely a design preference, but a fundamental engineering decision that directly impacts performance, computational complexity, robustness, and reliability. Islanded microgrid systems present distinct challenges such as the absence of a strong frequency reference and rapid power variations, necessitating control approaches specifically tailored to these conditions.

First, the use of multiple cascaded PI controllers inherently increases structural complexity and requires careful parameter tuning, which may pose challenges for practical implementation, especially under dynamic operating conditions. Second, continuous *dq* frame transformations introduce additional computational burdens that can limit scalability and real-time performance. Moreover, the reliance on PLL synchronization makes the method potentially sensitive to noise, parameter variations, and grid disturbances, especially during fast transients. In addition, the HCC framework is fundamentally based on an equivalent circuit model that involves output filter impedances of GFM and GFL inverters for control formulation. While such models can be effective in certain cases, they inherently tie the control performance to the precise knowledge of these parameters. Furthermore, the HCC implementation requires careful tuning of 12 control parameters for the PI controllers and relies heavily on precise knowledge of 4 physical parameters related to output filter impedances of parallel GFM and GFL inverters. This dependency on both numerous control parameters and accurate impedance values significantly increases design complexity and introduces potential performance vulnerabilities when actual system parameters deviate from design assumptions. In practice, however, system impedances often vary due to component tolerances, environmental factors, or unforeseen changes in operating conditions, potentially affecting control reliability and accuracy. The dependency on these parameters may therefore limit the method's robustness and applicability in more variable or uncertain environments.

It is also important to note that all tests and validations in [20] were conducted exclusively under grid-connected conditions. Therefore, the applicability of their method to islanded microgrids—where voltage and frequency regulation impose fundamentally different challenges—remains unexplored. This observation highlights a clear need for alternative control strategies that can address the unique demands of islanded operation modes, where robust, simpler, and practically implementable solutions are often essential.

In summary, although the HCC approach offers certain benefits within its original context, its reliance on complex control structures, impedance-dependent modeling, and PLL-based synchronization introduces significant limitations when considering broader or alternative applications, such as islanded microgrids. These aspects collectively underline a well-motivated research gap for developing alternative methods specifically tailored to such operational conditions.

B. RESEARCH CONTRIBUTIONS AND ARTICLE ORGANIZATION

Building upon the foundational concept of integrating GFM and GFL functionalities within a single inverter, as initially introduced by Lima and Watanabe in [20], this paper presents a unified hybrid control (UHC) framework specifically designed for islanded microgrid applications. While the underlying objective of combining both functionalities is shared with previous work, the proposed UHC introduces

a structurally distinct control architecture engineered to address the unique challenges of islanded operational environments, where the absence of a strong grid reference necessitates fundamentally different control approaches. The UHC framework employs a double-loop parallel control structure in the $\alpha\beta$ reference frame, utilizing a PR controller, thereby eliminating the need for PLL synchronization, which is particularly advantageous in islanded conditions. The selection of a PLL-free $\alpha\beta$-frame-based parallel control scheme therefore represents a technical solution aligned specifically with the operational characteristics and stability challenges of such systems. The primary contributions of this study can be summarized as follows:

1) PLL-FREE PARALLEL CONTROL ARCHITECTURE WITH SIMPLIFIED PARAMETERIZATION

This study proposes a dual-loop parallel control strategy operating entirely in the $\alpha\beta$ reference frame, eliminating the need for PLL synchronization and continuous dq transformations. While previous approaches like [20] utilize cascaded control structures, this parallel architecture is specifically designed for islanded microgrid applications, where frequency variations are more pronounced. The UHC implementation features a streamlined parameter set consisting of only three control parameters (two PR controller parameters and one active damping term), while other parameters represent physical system values. This architectural approach offers advantages in terms of reduced loop interdependencies and simplified parameter tuning for practical islanded microgrid applications, where operational simplicity can be particularly valuable.

2) SIMPLIFIED EQUIVALENT CIRCUIT MODELING APPROACH

The UHC framework employs a distinct equivalent circuit representation that combines a Thevenin equivalent model for the GFM portion with a current source model for the GFL portion. While this structural composition may appear superficially similar to previous equivalent circuit models such as in [20], it offers a fundamentally different approach to handling the current reference calculation of the GFL functional part. Specifically, the proposed model utilizes instantaneous power theory to directly determine the GFL current reference without relying on output filter impedance parameters. This approach reduces dependency on precise impedance matching assumptions that can be particularly challenging to maintain in practical islanded applications where component tolerances and operating conditions may vary. The resulting control architecture is designed to maintain consistent performance across a wider range of impedance variations, which may be advantageous in islanded microgrid environments where system parameters cannot always be precisely known or controlled.

3) COMPREHENSIVE PERFORMANCE VALIDATION FOR ISLANDED MICROGRIDS

The UHC framework integrates both GFM and GFL functionalities within a single voltage-controlled inverter, enhancing voltage and frequency stability while facilitating load sharing in islanded environments. Unlike previous work that primarily focused on grid-connected scenarios, this study provides extensive validation specifically tailored to islanded microgrid applications. The validation encompasses diverse operating conditions, including load changes, reference power variations, line outages, and short-circuit faults—scenarios that present unique challenges in islanded environments. These comprehensive tests demonstrate how the proposed architecture responds to the specific stability and reliability requirements of islanded microgrids, where maintaining consistent performance during transients and disturbances is particularly crucial.

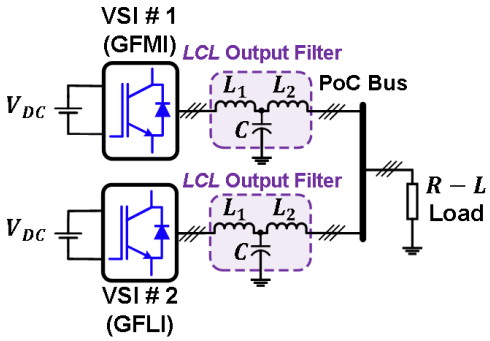

FIGURE 1. Single-line diagram of two VSIs operating as GFMI and GFLI with separate control systems connected in parallel in islanded mode.

4) IMPLEMENTATION EFFICIENCY AND RESOURCE OPTIMIZATION

The UHC approach offers several implementation advantages for practical islanded microgrid applications. By operating entirely in the $\alpha\beta$ reference frame without PLLs, the method reduces computational complexity and simplifies the parameter tuning process. The validation results demonstrate these computational benefits across various test scenarios. Additionally, the integration of both GFM and GFL functionalities within a single inverter unit contributes to more efficient resource utilization by reducing hardware requirements and minimizing dependency on large energy buffers. These characteristics are particularly valuable in islanded microgrid environments where hardware limitations, computational efficiency, and parameter sensitivity are common practical concerns. The overall architecture provides a balanced solution that addresses both the technical control requirements and practical implementation considerations for islanded microgrids.

Collectively, these engineering contributions demonstrate the practical advantages of the proposed UHC method for islanded applications, offering a structurally simple, robust, and effective control framework tailored to the specific operational needs of such systems.

This article is organized as follows. Section II reviews the performance of a parallel connection of a GFMI and a GFLI with independent controls under islanded conditions. Section III provides a detailed explanation of the operational and control principles of the proposed UHC scheme along

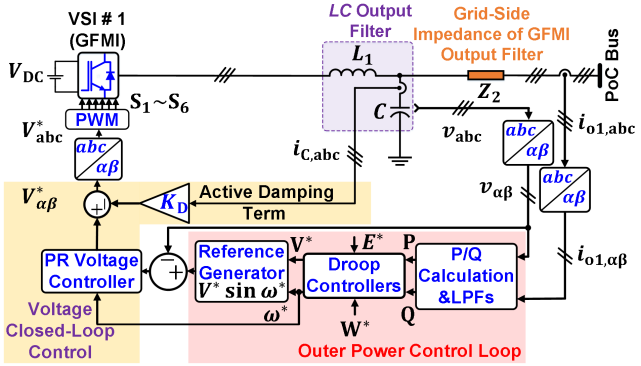

FIGURE 2. Control system for the GFMI based on the Clarke transform.

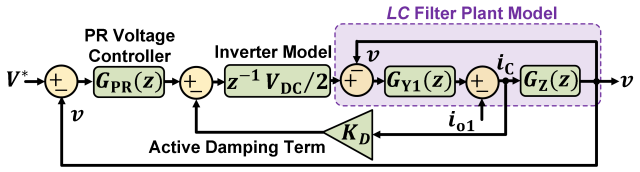

FIGURE 3. Block diagram of GFMI closed-loop voltage control system.

with its implementation. Section IV presents comprehensive simulation results, validating the effectiveness and feasibility of UHC under various application conditions on single- and multi-inverter systems operating in the islanded mode. Finally, the conclusions are presented in Section V.

II. CONNECTING GFMI AND GFLI IN PARALLEL IN ISLANDED MODE

To enhance the comprehension of the operational and control principles of the proposed UHC scheme for a single VSI, this section addresses the parallel performance of two VSIs acting as a GFMI and a GFLI with separate controls in the islanded mode, as shown in Figure 1. Considering the independent operation of the VSIs with distinct control objectives, their operating and control principles are examined separately in the following subsections.

A. OPERATION AND CONTROL PRINCIPLES OF GFMI

The GFMI, as a voltage-controlled inverter, controls the PoC voltage by adhering to a specified amplitude and frequency references. Additionally, GFMIs provide rapid grid support by autonomously responding to voltage and frequency deviations, thereby meeting grid code requirements [21]. A typical schematic of the GFMI control system based on Clarke transformation is shown in Figure 2. The output filter capacitor voltage is directly controlled in a GFMI or voltage-controlled IBR, and an *LCL* filter is typically used to mitigate the converter switching ripples [3]. In this case, L_2 is considered to be the grid-side impedance (Z_2). Despite the conventional use of a cascaded double-loop control structure for closed-loop voltage and current control in VSIs, the parameter design of these controllers remains complex [3], [22]. As demonstrated in [22], cascaded double-loop control can be reformulated into a parallel structure, offering an alternative perspective on its design complexities. This structure includes a single-loop control for accurate reference tracking and an internal virtual impedance term, ensuring well-damped output filter performance. The independent control of each term enhances flexibility and robustness and facilitates the tuning process for the controller parameters. Consequently, this study implemented GFMI and GFLI control systems based on this scheme in the $\alpha\beta$ frame.

To regulate the output voltage, GFMIs are primarily governed by reactive power-voltage amplitude and active power-frequency droop controllers [23]. This approach ensures a faster response by using only local measurements. The voltage amplitude and frequency references are automatically regulated based on the delivered active and reactive powers. Detailed explanations of the droop controller design, instantaneous active and reactive power calculation, and low-pass filter (LPF) implementation can be found in [23] and are not reiterated here. Owing to the challenges of using PI controllers for non-DC variable tracking [23], high-bandwidth PR controllers are primarily utilized in the $\alpha\beta$ frame, which is defined for the fundamental frequency as

$$G_{\mathrm{PR}}(s) = K_{\mathrm{pf}} + \frac{2K_{\mathrm{if}}\omega_{\mathrm{c}}s}{s^2 + 2\omega_{\mathrm{c}}s + (\omega^*)^2}, \tag{1}$$

Here, K_{pf} and K_{if} represent the fundamental proportional and resonant gains, respectively, while ω_{c} and ω^* denote the cutoff and fundamental angular frequencies, respectively. Dynamically tuning the resonant frequency via an active power-frequency droop controller (for GFMI) or a PLL (for GFLI), rather than keeping it constant, enables a PR controller to exhibit a high gain around the resonant frequency, ensuring accurate tracking. The proportional feedback of the filter capacitor current i_{C} is commonly considered as inner loop feedback to improve system damping and dynamic performance [22], [24], [25], [26], [27], as depicted in Figure 2. In Figure 3, a block diagram of the GFMI closed-loop voltage control system is depicted in the discrete-time domain (z-domain). The inverter was modeled as having a $V_{\mathrm{DC}}/2$ gain with a one-sample delay z^{-1} induced by the modulation process [28]. The discrete forms of the PR controller, represented as $G_{\mathrm{PR}}(z)$, filter inductor admittance as $G_{\mathrm{Y1}}(z)$, and filter capacitor impedance as $G_{\mathrm{Z}}(z)$, are derived using a Forward Euler (FE) transform with a sampling period of $T_{\mathrm{s}} = 1/f_{\mathrm{s}}$.

$$G_{\mathrm{PR}}(z) = K_{\mathrm{pf}} + \frac{2K_{\mathrm{if}}\omega_c T_s(z-1)}{(z-1)^2 + 2\omega_c T_s(z-1) + (\omega^* T_s)^2}. \tag{2}$$

$$G_{\mathrm{Y1}}(z) = \mathrm{FE}\left(\frac{1}{sL_1}\right) = \frac{T_{\mathrm{s}}}{L_1}\left(\frac{1}{z-1}\right). \tag{3}$$

$$G_{\mathrm{Z}}(z) = \mathrm{FE}\left(\frac{1}{sC}\right) = \frac{T_{\mathrm{s}}}{C}\left(\frac{1}{z-1}\right). \tag{4}$$

Referring to Figure 3, the performance of the GFMI closed-loop voltage control can be represented by a Thevenin equivalent circuit in the z-domain, as follows:

$$v(z) = G_{\mathrm{CL}}(z)V^* - Z_{\mathrm{o}}(z)i_{\mathrm{o1}}, \tag{5}$$

TABLE 1. Parameters of virtual parallel two-inverter system.

GFMI Parameters		
Symbol	**Description**	**Value**
V_{DC}	DC Link Voltage	800 V
f_{sw}	Switching Frequency	10 kHz
f_s	Sampling Frequency	10 kHz
ω^*	Nominal Frequency	$2\pi \times 50$ rad/s
$R_{L1}/L_1/C/R_{L2}/L_2$	*LCL* Filter	$0.05\Omega/1$ mH/25μF
$k_{pf}/k_{if}/\omega_C$	PR controller	0.1/500/2
K_D	Damping Term	5
GFLI Parameters		
Symbol	**Description**	**Value**
V_{DC}	DC Link Voltage	800 V
f_{sw}	Switching Frequency	10 kHz
f_s	Sampling Frequency	10 kHz
ω^*	Nominal Frequency	$2\pi \times 50$ rad/s
$R_{L1}/L_1/C$	*LC* Filter	$0.15\Omega/6$ mH/5μF
R_{L2}/L_2	Grid-side *L* Filter	$0.02\Omega/0.66$ mH/5μF
$k_{pf}/k_{if}/\omega_C$	PR controller	25/2500/2
K_D	Damping Term	1

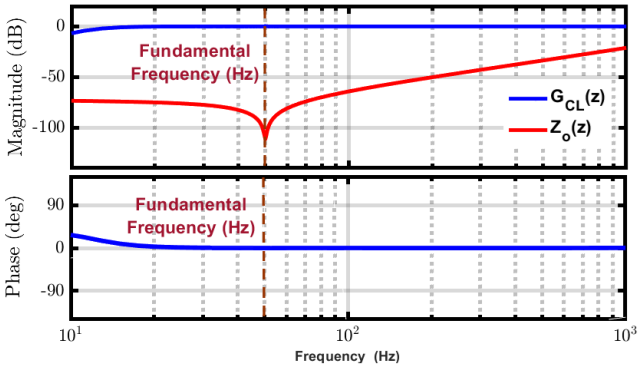

FIGURE 4. Bode diagrams of the closed-loop voltage tracking transfer function and closed-loop equivalent output impedance of the GFMI control system.

where V^*, v, $G_{CL}(z)$, and $Z_o(z)$ represent the reference voltage, filter capacitor voltage, closed-loop transfer function, and equivalent output impedance of GFMI control system, respectively. Therefore, applying Mason's theorem to Figure 3 allows the derivation of these closed-loop control parameters in the form of Equations (6) and (7).

$$G_{CL}(z) = \frac{v(z)}{V^*}\bigg|_{i_{o1}=0} = \frac{G_{PR}G_{Y1}G_Z z^{-1}V_{DC}/2}{1+G_{PR}G_{Y1}G_Z z^{-1}V_{DC}/2+K_D G_{Y1}z^{-1}V_{DC}/2+G_{Y1}G_Z}. \tag{6}$$

$$Z_o(z) = \frac{v(z)}{-i_{o1}}\bigg|_{V^*=0} = \frac{G_Z}{1+G_{PR}G_{Y1}G_Z z^{-1}V_{DC}/2+K_D G_{Y1}z^{-1}V_{DC}/2+G_{Y1}G_Z}. \tag{7}$$

Figure 4 depicts the Bode plots for $G_{CL}(z)$ and $Z_o(z)$ using the parameters listed in Table 1. At the fundamental frequency, the closed-loop voltage tracking transfer function exhibits unity gain and zero phase angle. Simultaneously, the magnitude of the closed-loop equivalent output impedance is zero at fundamental frequency. This ensures precise tracking of the voltage reference, allowing the GFMI to act as a voltage source with amplitude V^* and angular frequency ω^*. Although GFMI prioritizes grid voltage and frequency control, its integration with IBRs faces limitations. The control over the active and reactive powers of GFMI is not as precise as that of GFLI, given the automatic adjustments in power levels in response to variations in grid voltage and frequency. This discrepancy results in suboptimal performance for the RESs.

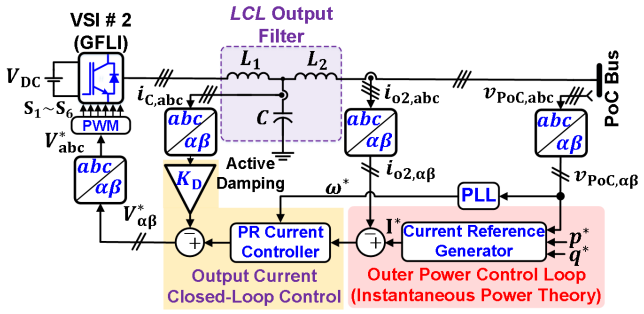

FIGURE 5. Control system for the GFLI based on the Clarke transform.

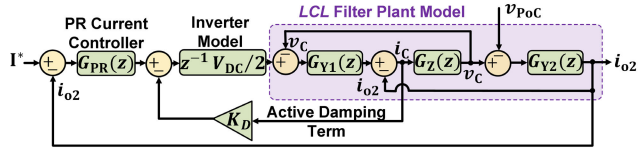

FIGURE 6. Block diagram of GFLI closed-loop current control system.

B. OPERATION AND CONTROL PRINCIPLES OF GFLI

The main goal of the GFLI control system as a current-controlled inverter is the precise and prompt tracking of specified references for both active and reactive powers. To ensure an accurate power exchange with the grid, it incorporates a PLL for synchronization with the voltage at the PoC. In addition, it uses a rapid current control loop to adjust the output current according to the specified reference power levels. Figure 5 illustrates the GFLI control system based on the $\alpha\beta$ reference frame, where the active and reactive power references are converted to synchronized output current references using instantaneous power theory [29].

$$\begin{bmatrix} i^*_\alpha \\ i^*_\beta \end{bmatrix} = \frac{1}{v^2_{PoC,\alpha}+v^2_{PoC,\beta}} \begin{bmatrix} v_{PoC,\alpha} & v_{PoC,\beta} \\ v_{PoC,\beta} & v_{PoC,\beta} \end{bmatrix} \begin{bmatrix} p^* \\ q^* \end{bmatrix}. \tag{8}$$

Figure 6 illustrates block diagram of the GFLI closed-loop current control system in the z-domain. The closed-loop current control performance in the GFLI can be represented by a Norton equivalent circuit as:

$$i_{o2}(z) = G_{CLC}(z)I^* - Y_o(z)v_{PoC}. \tag{9}$$

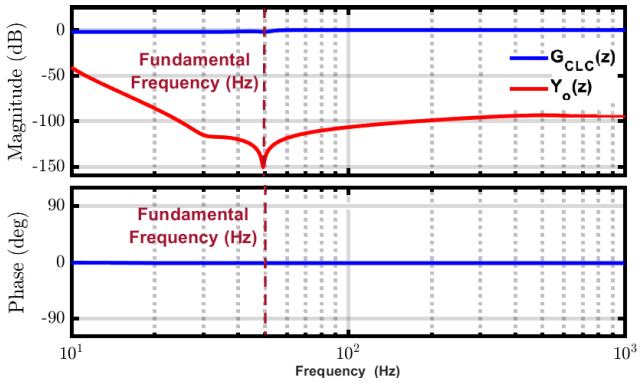

FIGURE 7. Bode diagrams of the closed-loop current tracking transfer function and closed-loop equivalent output admittance of the GFLI control system.

where $G_{\mathrm{CLC}}(z)$ and $Y_{\mathrm{o}}(z)$ denote the closed-loop transfer function and equivalent output admittance of the GFLI control system, respectively. By applying Mason's theorem in Figure 6, these parameters can be deduced as follows:

$$G_{\mathrm{CLC}}(z) = \left.\frac{i_{\mathrm{o2}}(z)}{\mathrm{I}^*}\right|_{v_{\mathrm{PoC}}=0} = \frac{G_{\mathrm{PR}}G_{\mathrm{Y1}}G_{\mathrm{Z}}G_{\mathrm{Y2}}z^{-1}V_{\mathrm{DC}}/2}{1+G_{\mathrm{PR}}G_{\mathrm{Y1}}G_{\mathrm{Z}}G_{\mathrm{Y2}}z^{-1}V_{\mathrm{DC}}/2+K_{\mathrm{D}}G_{\mathrm{Y1}}z^{-1}V_{\mathrm{DC}}/2+G_{\mathrm{ZY}}}. \tag{10}$$

$$Y_{\mathrm{o}}(z) = \left.\frac{io2(z)}{-v_{\mathrm{PoC}}}\right|_{i^*=0} = \frac{G_{\mathrm{Y2}}(1+K_{\mathrm{D}}G_{\mathrm{Y1}}z^{-1}V_{\mathrm{DC}}/2+G_{\mathrm{Z}}G_{\mathrm{Y1}})}{1+G_{\mathrm{PR}}G_{\mathrm{Y1}}G_{\mathrm{Z}}G_{\mathrm{Y2}}z^{-1}V_{\mathrm{DC}}/2+K_{\mathrm{D}}G_{\mathrm{Y1}}z^{-1}V_{\mathrm{DC}}/2+G_{\mathrm{ZY}}}. \tag{11}$$

where $G_{\mathrm{ZY}} = G_{\mathrm{Z}}(G_{\mathrm{Y1}} + G_{\mathrm{Y2}})$. Figure 7 displays the Bode plots for $G_{\mathrm{CLC}}(z)$ and $Y_{\mathrm{o}}(z)$ based on the parameters listed in Table 1. At the fundamental frequency, the closed-loop current tracking transfer function exhibits unity gain and zero-phase angle. Additionally, the closed-loop equivalent output admittance has a magnitude of zero at the fundamental frequency. These characteristics ensure precise tracking of the current reference when implementing the control scheme depicted in Figure 5. Consequently, the GFLI operates as a current source with an amplitude of I* and maintains synchronization with the PoC voltage. Nevertheless, GFLI relies on a pre-established and relatively stable power grid, limiting its ability to control the grid voltage and frequency in scenarios with weak or unstable grids. During transient or disturbance events that lead to fluctuations in grid voltage and frequency, a GFLI maintains its predetermined active and reactive power objectives and cannot respond quickly enough to effectively mitigate these issues, as it depends on accurate voltage and frequency measurements for proper operation. Therefore, it is crucial to implement supplementary control strategies to enable grid-support functionalities for GFLI.

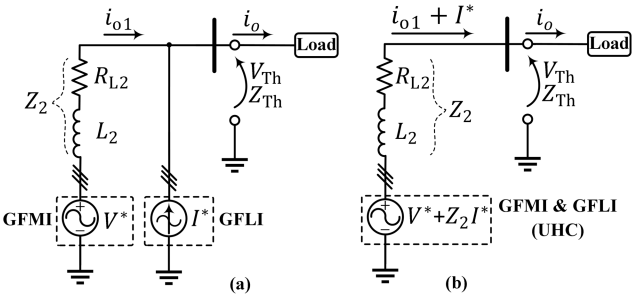

FIGURE 8. A single-line diagram represents (a) the virtual system composed of two VSIs (GFMI and GFLI) and (b) the actual system featuring a single voltage-controlled VSI governed by UHC, exhibiting identical behavior to the virtual system.

III. PROPOSED UNIFIED HYBRID CONTROL SCHEME

Well-designed control schemes transform the GFMI into a voltage source and the GFLI into a current source at their AC terminals. The GFMI was connected to the PoC through the grid-side impedance of its output filter, as shown in Figure 8(a). While the equivalent circuit approach used in this study (a Thevenin equivalent model for the GFM portion combined with a current source model for the GFL portion) may appear structurally similar to previous approaches, such as in [20], there are notable differences in the implementation that are specifically relevant for islanded applications. The model in [20] employs dual Thevenin equivalent circuits with certain assumptions about output filter impedances, as noted in [20]. In contrast, for islanded microgrid applications, the proposed approach in this study calculates the GFL current reference directly using instantaneous power theory without relying on output filter impedance parameters. This structural difference leads to a distinct control formulation that is specifically designed for the unique challenges of islanded operation, where voltage and frequency stability are particularly critical. A detailed numerical comparison between these approaches is beyond the scope of this paper, as they target different operational contexts. In this configuration, an equivalent circuit can be considered from the PoC perspective, where a single voltage-controlled VSI replicates operational characteristics similar to the scenario of two distinct VSIs interconnected in parallel in the islanded mode, as portrayed in Figure 8(b). In this manner, *a VSI controlled via the UHC strategy becomes a viable means to emulate the performance of two hypothetical virtual VSIs—a GFMI and a GFLI— operating simultaneously in parallel.* This implies that the open-circuit voltage (V_{Th}), equivalent impedance (Z_{Th}), and total current (i_{o}) observed at the PoC are identical in both scenarios.

A. ANALYTICAL CIRCUIT AND MATHEMATICAL FORMULATION

Determining the V_{Th} and Z_{Th} values is crucial to realize a UHC-based VSI that mirrors the behavior of two virtual parallel VSIs from the PoC standpoint, serving as an equivalent voltage source in series with an equivalent impedance (Figure. 8(b)). By applying Thevenin's theorem [30] to the

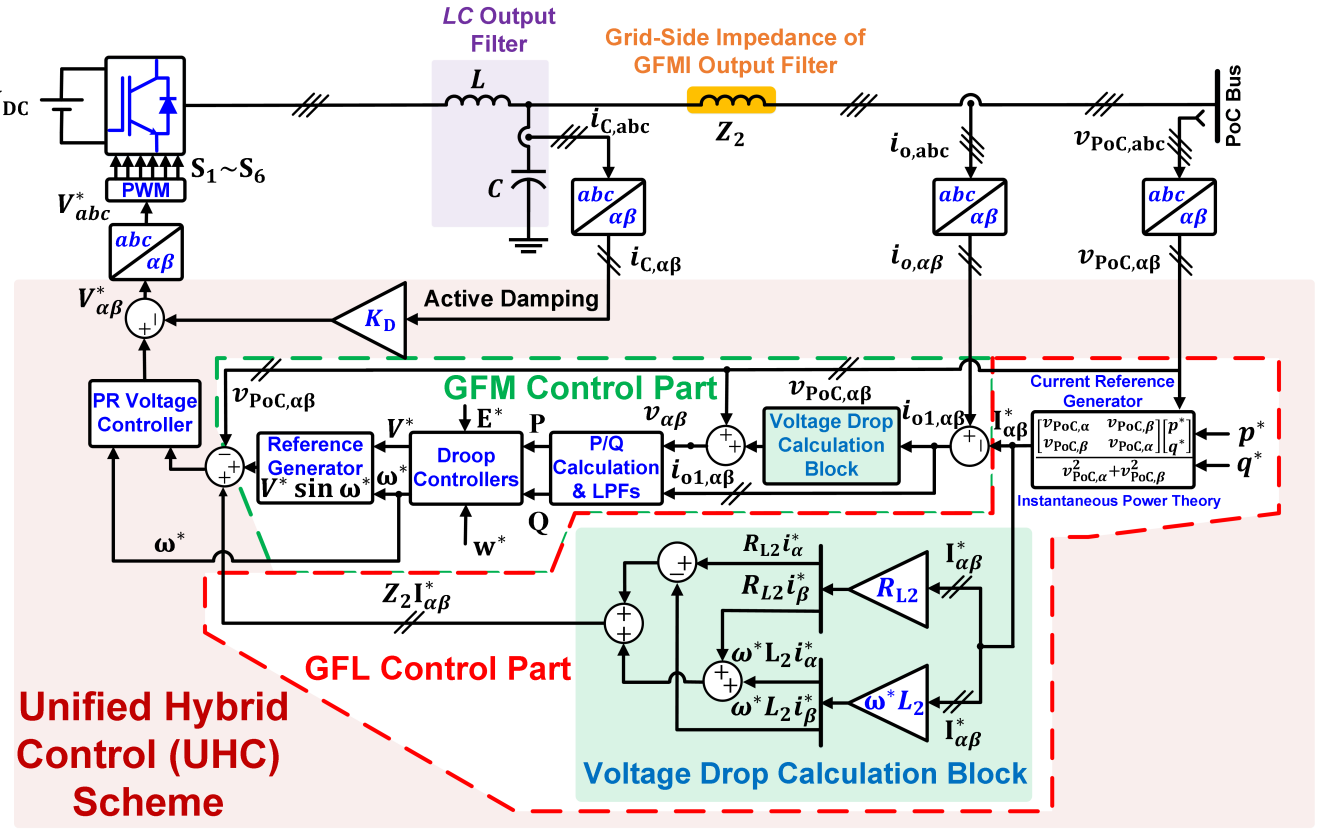

FIGURE 9. The proposed UHC scheme for a single voltage-controlled VSI.

configuration shown in Figure 8(a), the following expressions are derived:

$$v_{oc} = V_{Th} = V^* + Z_2 I^*, \tag{12}$$
$$Z_{Th} = Z_2, \tag{13}$$
$$i_{o1} = i_o - I^*, \tag{14}$$

Here, the variables v_{oc} (PoC open-circuit voltage), V^* (GFMI reference voltage), I^* (GFLI reference current), i_o (total current flowing through the PoC), i_{o1} (GFMI output current), and Z_2 (GFMI grid-side impedance) are defined. The equivalent circuit of the UHC-based single VSI, resulting from the integration of a GFMI and a GFLI in parallel in the virtual system, can be understood through Figure 8 and Equations (12)-(14). This forms the foundation of the proposed UHC scheme. The key idea is that V_{Th} is established by adding the GFMI reference voltage to the voltage drop across the grid-side impedance of the GFMI output filter induced by the GFLI reference current in the mimicked virtual two-inverter system (see Equation (12)). Additionally, the GFMI output current, which is needed to derive the GFMI reference voltage, can be back-calculated by subtracting the GFLI reference current from the measured total current at the PoC (see Equation (14)). The equivalent series impedance is considered equal to the grid-side impedance of the GFMI output filter (see Equation (13)).

B. IMPLEMENTATION OF THE UHC METHOD

As shown in Figure 8(b), the goal of implementing the UHC technique on a single voltage-controlled VSI is to replicate the performance of a virtual system consisting of a GFMI and GFLI operating in parallel. Figure 9 illustrates the implementation of the UHC method in the $\alpha\beta$ reference frame. In this scheme, the control system takes inputs from the voltage and current measurements at the PoC and the output filter capacitor current. The UHC system output then serves as the reference voltage for the VSI AC terminals. The following outlines the process of implementing the UHC approach in a single VSI, based on the two-inverter virtual system:

STEP 1
CALCULATION OF REFERENCE CURRENT I^*

According to Equation (12), calculating V_{Th} for the UHC-based VSI involves determining the GFLI reference current in the virtual two-inverter system. This process begins by measuring the PoC voltage, which is identical in both the systems. After converting v_{PoC} into the $\alpha\beta$ frame and considering the desired reference values for active and reactive powers, these parameters are input into the *"Current Reference Generator"* block. This block then computes I^*, emulating the virtual GFLI performance as outlined in Equation (8).

STEP 2
CALCULATION OF VOLTAGE DROP $Z_2\mathbf{I}^*$

As seen in Figure 9, the *"Voltage Drop Calculation"* block is utilized in the UHC scheme to determine the voltage drop across the grid-side impedance of the GFMI output filter caused by the GFLI reference current in the emulated virtual two-inverter system. In this block, the desired voltage drop components in the $\alpha\beta$ frame are derived as

$$Z_2\mathbf{I}^*_{\alpha\beta} = \begin{bmatrix} R_{L2} & -\omega^* L_2 \\ \omega^* L_2 & R_{L2} \end{bmatrix} \begin{bmatrix} i^*_\alpha \\ i^*_\beta \end{bmatrix} = \begin{bmatrix} R_{L2} i^*_\alpha - \omega^* L_2 i^*_\beta \\ \omega L_2 i^*_\alpha + R_{L2} i^*_\beta \end{bmatrix}. \quad (15)$$

The voltage drop $Z_2\mathbf{I}^*$ forms a part of V_{Th} that needs to be generated within the UHC scheme (see Equation (12)).

STEP 3
CALCULATION OF OUTPUT CURRENT I_{O1} *AND FILTER CAPACITOR VOLTAGE* V

Referring to Equation (12), another component of V_{Th} in the UHC scheme corresponds to the GFMI reference voltage (V^*) in the virtual two-inverter system. As explained in Section II, Subsection A, generating V^* requires calculating both the GFMI output current (i_{o1}) and its filter capacitor voltage (v). However, in the single VSI structure, the available measurements are v_{PoC} and total current (i_{o}), which correspond to the two-inverter virtual system. Therefore, as illustrated in Figure 9, to back-calculate i_{o1}, Equation (14) is employed. To determine v, the following equation is used:

$$v = v_{\text{PoC}} + Z_2 i_{\text{o1}}. \quad (16)$$

Accordingly, the voltage drop $Z_2 i_{\text{o1}}$ forms a part of v that must be generated within the UHC scheme (refer to Figure 9).

STEP 4
CREATION OF THE REFERENCE VOLTAGE V_{TH}

By applying v and i_{o1} to the sequential control structure, comprising the *"P/Q Calculation and LPFs"*, *"Droop Controllers"*, and *"Reference Generator"* blocks, as shown in Figure 9, V^* can be derived. Subsequently, as specified in Equation (12), by adding V^* to the result obtained in the second step ($Z_2\mathbf{I}^*$), V_{Th} is generated.

Ultimately, by employing PR controller-based voltage closed-loop control, the voltage-controlled VSI terminal voltage is precisely regulated to ensure that the measured v_{PoC} accurately tracks V_{Th}. This approach efficiently takes advantage of the performance benefits of both the GFMI and GFLI simultaneously in the form of a single VSI with a UHC approach for islanded microgrid applications. From the PoC perspective, it appears as if there is a GFMI and GFLI connected in parallel, each with its own control. In reality, however, a single UHC-based VSI seamlessly integrates GFL functionality into its GFM functionality for islanded operation.

While utilizing the $\alpha\beta$ frame to eliminate PLL dependency is a recognized principle in inverter control, the proposed UHC control architecture extends beyond this aspect. As illustrated in Figure 9, the structural design of the UHC method incorporates a parallel dual-functionality control system specifically optimized for islanded applications. This architecture consists of a GFL control section that utilizes instantaneous power theory for current reference generation and direct voltage drop calculation, alongside a GFM control section with droop controllers. This approach employs a limited number of control parameters (three parameters: two for the PR controller and one for damping), and relies on directly measured inputs (voltage and current at PoC). These characteristics are particularly relevant for islanded systems that face challenges such as the absence of a strong frequency reference and rapid load variations. The effectiveness of this control structure under various challenging islanded scenarios is demonstrated through multiple simulation studies presented in the following sections.

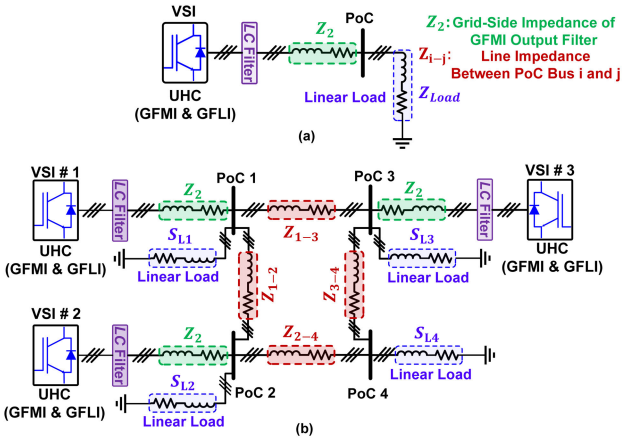

FIGURE 10. Schematic of the simulated islanded power systems. (a) UHC-enabled single VSI, (b) Four-bus stand-alone power system utilizing UHC-equipped VSIs.

IV. COMPREHENSIVE SIMULATION STUDIES FOR VERIFICATION OF THE PROPOSED UHC STRATEGY

The effectiveness, resilience, and robustness of proposed UHC scheme were evaluated using two comprehensive simulation studies. The first study focused on a UHC-based VSI connected to a linear load in the islanded mode (Figure 10(a)). This study aimed to assess the capability of the UHC to emulate the distinct functions of GFMI and GFLI within a unified framework. In the second study, an extensive simulation was conducted on a four-bus stand-alone power distribution system (Figure 10(b)), further validating the versatility and flexibility of UHC within broader power system contexts. The interconnected system featured typical distinct LV line impedances, with three UHC-based VSIs supplying loads. Both studies, conducted in the discrete-time domain using MATLAB/Simulink, accurately simulated real-world conditions by incorporating control system delays, considering both computation and pulse width modulation delays. The model parameters and simulation details for the case studies are provided in Tables 2, 3, and 4, exploring three operational scenarios.

SCENARIO 1

Impact of Sudden Changes in Load Levels.

TABLE 2. Parameters of the simulated systems.

Symbol	Description	Value
V_{DC}	DC Link Voltage	800 V
f_{sw}	Switching Frequency	10 kHz
f_s	Sampling Frequency	10 kHz
E^*	Network L-L RMS Voltage	400 Vrms
W^*	Nominal Frequency	$2\pi \times 50$ rad/s
P_n	Rated Active Power	10kW (GFMI+GFLI)
Q_n	Rated Reactive Power	4.4kVAR (GFMI+GFLI)
$R_L/L/C$	LC Filter	0.05Ω/2 mH/2.5μF
Z_2	GFMI Grid-Side Impedance	50 $m\Omega$+j0.628 Ω
K_{iP}	Integral Frequency Droop	0.0002513 W/rd (0.4%)
K_{pP}	Proportional Frequency Droop	0.00005027 Ws/rd
K_{pQ}	Proportional Amplitude Droop	0.005938 VAR/V (4%)
$k_{pf}/k_{if}/\omega_C$	PR controller	0.1/50/2
K_D	Damping Term	5
Z_{1-2}	Line Impedance	0.15 Ω+j0.05 Ω
Z_{1-3}	Line Impedance	0.18 Ω+j0.06 Ω
Z_{2-4}	Line Impedance	0.2 Ω+j0.067 Ω
Z_{3-4}	Line Impedance	0.1 Ω+j0.03 Ω

TABLE 3. Case studies for UHC-based single VSI system.

Sudden Load Changes and Variations in Reference Powers		
Case Number	S_{Load}	$p^* + jq^*$
Case 1	5kW+j2.2kVAR	2.5kW+j1.1kVAR
Case 2	6.25kW+j2.75kVAR	2.5kW+j1.1kVAR
Case 3	3.75kW+j1.65kVAR	2.5kW+j1.1kVAR
Case 4	4.75kW+j2.4kVAR	3.5kW+j1.87kVAR

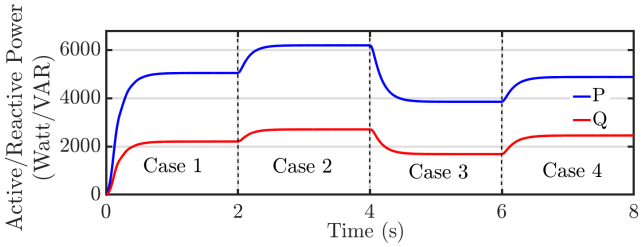

FIGURE 11. Active and reactive powers at the PoC bus in the UHC-enabled single VSI system under various operational cases.

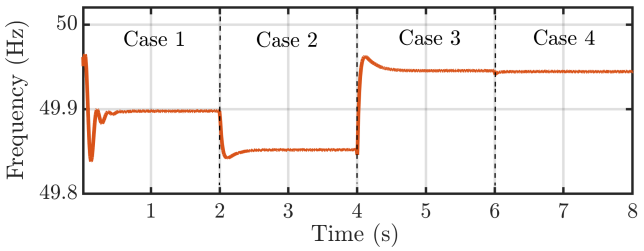

FIGURE 12. System frequency response in the UHC-enabled single VSI system under various operational cases.

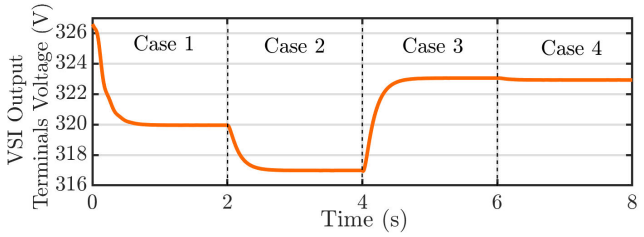

FIGURE 13. Phase peak voltage of the VSI terminals in the UHC-enabled single VSI system under various operational cases.

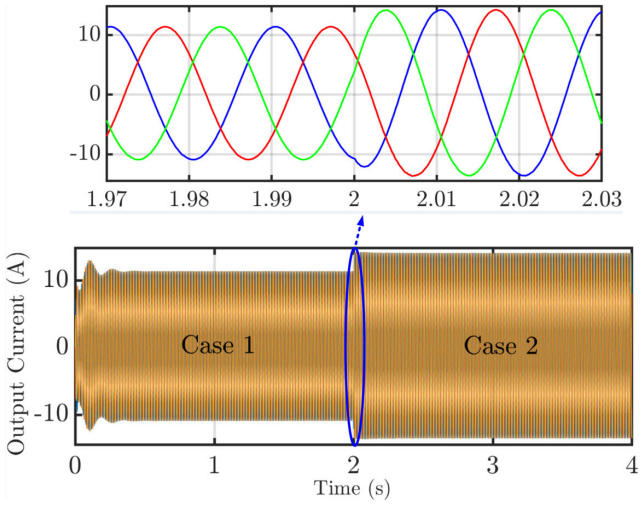

FIGURE 14. Output current in the UHC-enabled single VSI system during a sudden voltage drop and phase jump scenario.

SCENARIO 2

Effect of Variation in Reference Powers.

SCENARIO 3

Impact of Line Outage and Reconnection.

A. UHC-ENABLED SINGLE VSI

SCENARIO 1

Impact of Sudden Changes in Load Levels.

In this scenario, the objective is to validate the steady-state and transient performance characteristics, along with the robustness of the proposed UHC scheme under various levels and sudden changes in load for a VSI in an islanded operation. To achieve this, the system in Figure 10(a) was exposed to three distinct sudden loading conditions outlined in Table 3, denoted as cases and sequentially presented for analysis.

- **Case 1** ($0s \leq t \leq 2s$)

As shown in Table 3, during this interval, the reference powers for the GFLI functional part are set to ensure that it operates at 50% of its rated capacity. To validate the effectiveness of UHC in achieving desirable steady-state performance within a single voltage-controlled VSI, mirroring the virtual parallel operation of a GFMI and a GFLI, the powers delivered to the PoC must exactly match the sum of the reference power tracked by the virtual GFLI part and the generated power proportional to the residual load demand by the virtual GFMI part operation. Figure 11 confirms the precise tracking of the output reference powers achieved through output current control, utilizing the inherent advantages of a GFLI. Consequently, the UHC-based VSI delivers 2.5 kW and 1.1 kVAR associated with the GFLI functional part. The illustration also demonstrates accurate load sharing based on the remaining load level, effectively replicating the

TABLE 4. Case studies for four-bus stand-alone system utilizing UHC-equipped VSIs.

Impact of Sudden Load Change in S_{L4}, Variations in VSIs Reference Powers, and Z_{2-4} Line Outage and Reconnection			
Case 1	**Case 2**	**Case 3**	**Case 4**
$S_{L1,L2,L3}$ = 5kW+j2.2kVAR	$S_{L1,L2,L3}$ =5kW+j2.2kVAR	$S_{L1,L2,L3}$ =5kW+j2.2kVAR	$S_{L1,L2,L3}$ =5kW+j2.2kVAR
S_{L4} = 1.8kW+j0.9kVAR	S_{L4} =2.25kW+j1.125kVAR	S_{L4} =2.25kW+j1.125kVAR	S_{L4} =2.25kW+j1.125kVAR
$p_1^* + jq_1^*$ = 2.5kW+j1.1kVAR	$p_1^* + jq_1^*$ =1.5kW+j0.66kVAR	$p_1^* + jq_1^*$ =1.5kW+j0.66kVAR	$p_1^* + jq_1^*$ =1.5kW+j0.66kVAR
$p_2^* + jq_2^*$ = 3.5kW+j1.54kVAR	$p_2^* + jq_2^*$ =2.5kW+j1.1kVAR	$p_2^* + jq_2^*$ =2.5kW+j1.1kVAR	$p_2^* + jq_2^*$ =2.5kW+j1.1kVAR
$p_3^* + jq_3^*$ = 2kW+j0.88kVAR	$p_3^* + jq_3^*$ =3kW+j1.32kVAR	$p_3^* + jq_3^*$ =3kW+j1.32kVAR	$p_3^* + jq_3^*$ =3kW+j1.32kVAR

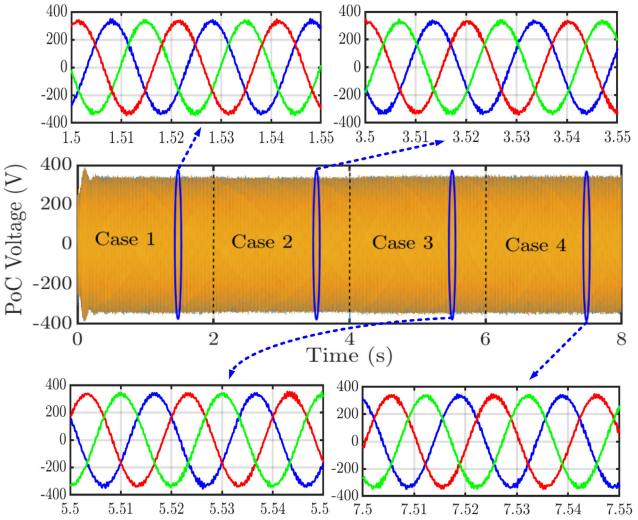

FIGURE 15. PoC voltage in the UHC-enabled single VSI system under various operational cases.

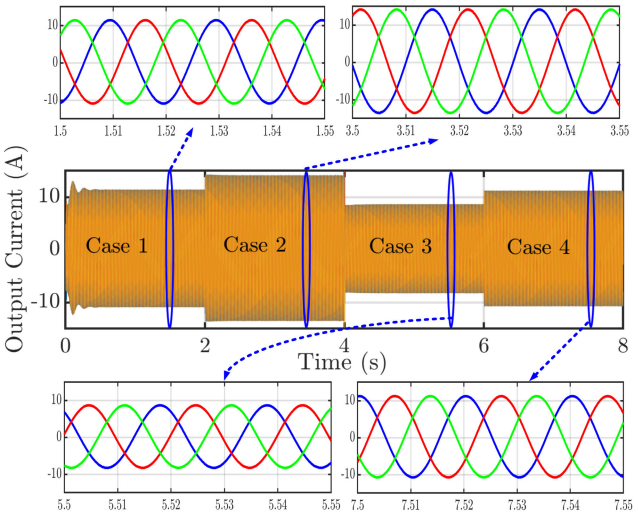

FIGURE 16. Output current in the UHC-enabled single VSI system under various operational cases.

operational characteristics of a GFMI functioning at 50% of its rated capacity. As a result, the UHC-based VSI delivers 2.5 kW and 1.1 kVAR associated with the GFM functional part. Accordingly, Figure 12 shows a 0.1 Hz decrease in the system frequency, which is attributed to the frequency droop characteristic and the active power value generated by the

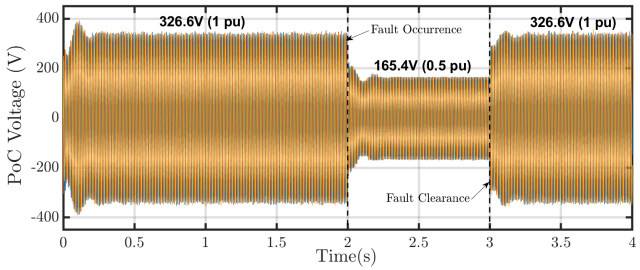

FIGURE 17. PoC voltage profile in the UHC-enabled single VSI system during a three-phase short-circuit fault event.

virtual GFMI part. Furthermore, as depicted in Figure 13, due to the amplitude droop characteristic and reactive power supplied by the virtual GFMI part, the peak voltage at the VSI output terminals relative to its rated value has reduced by 6.5 volts. Therefore, by utilizing a UHC-based single VSI, the system effectively achieves the primary advantages of both GFMI (precise frequency and voltage regulation) and GFLI (accurate tracking of output reference powers) simultaneously.

- **Case 2** ($2s \leq t \leq 4s$)

In Case 2, as outlined in Table 3, an abrupt load level change is applied. Similar to Case 1, the reference powers for the GFLI functional part remain constant. Figure 11 illustrates that despite the transient load level change, the UHC-based single VSI achieves rapid and accurate tracking of the output reference powers, alongside precise load sharing based on the remaining load level. In this case, the GFMI functional part operates at 75% of its rated capacity under steady-state conditions. Furthermore, the ability of the control approach to adjust the system frequency, as depicted in Figure 12, verifies the compatibility of the UHC with dynamic load changes while ensuring frequency stability. The UHC-enabled VSI also demonstrates its synthetic inertia capability by seamlessly adapting to sudden load changes, ensuring a controlled frequency response for load transient stability. As seen in Figure 13, the amplitude/reactive power droop characteristic of the virtual GFMI section induces a controlled 9.8 V reduction in the peak voltage of the output terminals. A sudden change in the reactive load leads to a phase shift and a voltage drop. To investigate the effectiveness of the proposed UHC method in the management of current limitations, a voltage drop of more than 2% compared to the nominal (approximately one percent of the voltage drop compared to Case 1) has been applied in Case 2, with a sudden increase in reactive load power of 550 VAR

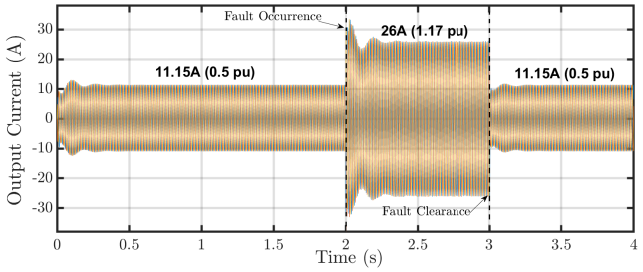

FIGURE 18. Output current in the UHC-enabled single VSI system during a three-phase short-circuit fault event.

and keeping the reference reactive power constant for GFL operation similar to case 1 (see Table 3). The creation of this voltage drop scenario can be seen in Figure 13 in the time interval of 2 to 4 seconds (Case 2) under operational scenario 1. By increasing this amount of reactive power for the GFMI functional part of the UHC-based VSI, an abrupt phase change of approximately 10 degrees occurs in case study 2. Figure 14 illustrates the output current waveform of the UHC-based VSI during this sudden voltage drop and phase change induced by reactive load variations in Case 2. The VSI equipped with UHC, effectively confines the current within permissible limits during these transient events, thereby preventing potential damage and ensuring stability. These results confirm the efficacy of the transient response control, showcasing the robustness of the proposed strategy under severe disturbances. This adaptive response ensures the inverter operates within safe operational parameters, contributing to system stability during these transient conditions. This is because, utilizing the UHC method, a portion of the output power from the UHC-based voltage-controlled VSI is supplied by the GFL functional part. This integration enables flexible control of the power delivered by the GFM operational part of the VSI, thus preventing the current from exceeding the permissible limit. Using the UHC strategy, the seamless integration of GFM and GFL functionalities within a single VSI effectively acts as a current limiter. Figures 15 and 16 confirm the robust performance of the UHC in preserving high-quality current and voltage waveforms even during dynamic load changes. In this scenario, the system response to a sudden load change was analyzed to rigorously evaluate the UHC's effectiveness in ensuring load transient stability and local grid support capability during dynamic events.

To evaluate the performance of the UHC method in current limitation management under more severe disturbances, another simulation was conducted considering a three-phase short-circuit fault at the load terminals. This fault occurs at $t = 2s$ and is cleared at $t = 3s$, causing a significant voltage drop of approximately 50% of the nominal value. During severe transient events, such as substantial voltage drops, in addition to reducing the reference reactive power of the GFL functional part to zero, the voltage-reactive power droop control coefficient is dynamically adjusted based on the voltage drop magnitude. This dual adjustment ensures that the output current remains within permissible limits. The theoretical framework for this dynamic adjustment is based on the principle of maintaining a balanced power exchange and stable voltage regulation under varying load and fault conditions. The nominal peak current is approximately 22.3 A. Thus, a range of 1.1 to 1.3 per unit corresponds to a current range of 24.53 to 29 A. These calculations are based on a nominal active power of 10 kW, a nominal reactive power of 4.4 kVAR, and a line-to-line voltage of 400 V. Figure 17 shows the voltage profile during the fault event, and Figure 18 illustrates the output current during this event. It can be seen that the current is effectively limited within the specified range of 24.53 to 29 A. After the fault is cleared at $t = 3s$, the system returns to its pre-fault condition without any instability. In cases of less severe voltage drops and phase jumps, current limitation management can be achieved solely by controlling the reference reactive power of the GFL functional part within the UHC scheme. This is demonstrated by the results shown in Figure 14, where only the reference reactive power adjustment is sufficient to manage the current within safe limits under less severe conditions. By employing these strategies, the UHC method ensures robust performance and stability under various operating conditions, from minor disturbances to severe faults. It should be noted that the primary focus of this article is on presenting a comprehensive hybrid control method to simultaneously integrate the operational advantages of GFMI—grid voltage and frequency regulation and microgrid support capability—and GFLI, precisely tracking reference powers. Consequently, there is potential for integrating more optimized current-limiting methods such as predictive current control or adaptive current-limiting strategies into the proposed UHC design.

- **Case 3** ($4s \leq t \leq 6s$)

During this interval, another sudden change in the load level occurs (see Table 3). As before, the reference powers for the GFLI functional part remain unchanged. The UHC-enabled single VSI handles sudden load variations, demonstrating its capability in accurately tracking reference powers and achieving precise load sharing (see Figure 11). In Figure 12, the UHC demonstrates controlled frequency regulation through frequency droop, authenticating its proficiency in managing dynamic load changes while maintaining frequency stability. This study also accentuates the UHC synthetic inertia capability, as evidenced by the controlled response in the frequency regulation. The controlled 3.3 V reduction in the peak voltage of the output terminals shown in Figure 13 confirms the voltage regulation and stability under dynamic conditions based on the amplitude droop coefficient. The results obtained in case studies 2 and 3 verify the effectiveness of the UHC in handling sudden load changes, ensuring robust transient stability, local grid supportability, and maintaining high-quality waveforms.

SCENARIO 2

Effect of Variation in Reference Powers.

- **Case 4** ($6s \leq t \leq 8s$)

In this scenario, a sudden change in the reference powers is applied (see Table 3). The active power reference for the

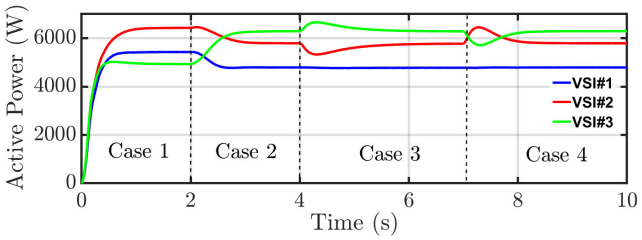

FIGURE 19. Active powers at the PoC buses in the four-bus standalone system with UHC-equipped VSIs under various operational cases.

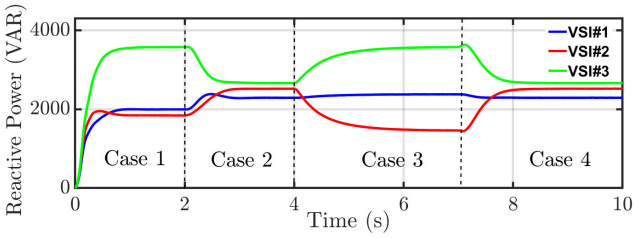

FIGURE 20. Reactive powers at the PoC buses in the four-bus standalone system with UHC-equipped VSIs under various operational cases.

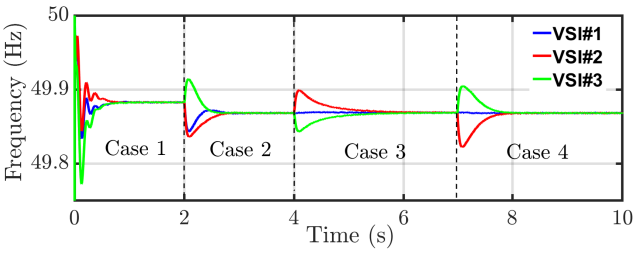

FIGURE 21. System frequency response in the four-bus standalone system with UHC-equipped VSIs under various operational cases.

GFLI functional part is adjusted to 70% of its rated capacity, and the reactive power reference varies to 85% of its rated capacity under steady-state conditions. Meanwhile, the load levels remain unchanged, similar to Case 3. As shown in Figure 11, the UHC-enabled single VSI demonstrates the capability to adapt to sudden variations in reference powers, achieving fast and precise tracking along with accurate load sharing. Figures 12 and 13 exhibit the controlled regulation of frequency and voltage and validate the accuracy of the UHC in islanded network support based on droop coefficients. Despite variations in the reference powers, the system maintains stability with consistent load levels and adheres to the initial frequency and voltage settings, demonstrating UHC performance. Besides, Figures 15 and 16 depict high-quality waveforms even with variations in the reference powers. In conclusion, the results confirm the efficacy of UHC in integrating GFM and GFL capabilities within a single VSI. The demonstrated resilience, stability, and performance characteristics verify the effectiveness of UHC, establishing its applicability for diverse tasks in islanded power systems.

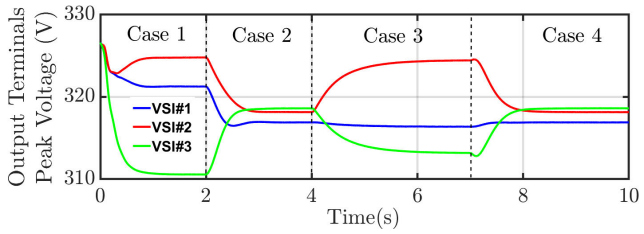

FIGURE 22. Phase peak voltage of the VSIs output terminals in the four-bus standalone system with UHC-equipped VSIs under various operational cases.

B. FOUR-BUS STANDALONE SYSTEM WITH UHC-EQUIPPED VSIs

SCENARIOS 1 AND 2

Impact of Sudden Load Change in S_{L4} and Variations in VSIs Reference Powers.

This case study aims to evaluate the versatility, robustness, and performance of the proposed UHC within the context of broader power systems, as illustrated in Figure 10(b). This islanded power system was subjected to a sudden load change in S_{L4} and simultaneous variations in the VSIs reference powers, as outlined in Table 4.

- **Case 1** ($0s \leq t \leq 2s$)

Within this time frame, the reference powers for the GFLI functional part of VSI#1, VSI#2, and VSI#3 are set at 50%, 70%, and 40% of their rated capacities, respectively. These configurations are detailed in Table 4. In this topology, it is crucial to validate the efficacy of the UHC scheme in achieving consistent steady-state performance and efficient power flow management within a multi-VSI setup operating in the islanded mode. Each inverter emulates the parallel operation of a GFMI and GFLI. To evaluate this, the injected powers in each PoC must precisely match the sum of the reference powers tracked by the virtual GFLI section of each VSI and the generated power proportional to the residual load demand resulting from the virtual GFMI section of each VSI, considering the frequency/voltage droop coefficient. As illustrated in Figures 19 and 20, the UHC strategy ensures precise tracking of reference powers and accurate load sharing among VSIs, effectively managing the power flow to address simultaneously diverse load levels and islanded grid requirements. As expected and illustrated in Figure 19, considering the rated power and frequency droop coefficients of the VSIs, the active powers obtained from the GFMI operational part of each VSI are accurately and equally shared in the steady-state, despite the mismatched line impedances. This assertion can be validated by subtracting the reference active power value tracked by the GFLI operational part of each VSI from the active power at the PoC bus of each VSI (refer to Figure 1): VSI#1 (5.43kW-2.5kW=2.93kW), VSI#2 (6.43kW-3.5kW=2.93kW), VSI#3 (4.93kW-2kW=2.93kW). Nevertheless, Figure 20 illustrates that accurate sharing of steady-state reactive power between VSIs is compromised due to interface impedance mismatches, considering the GFMI power ratings and amplitude

droop coefficients. Furthermore, as seen in Figure 21, consistent with the frequency droop characteristic (0.4%), the rated active power of the GFMI part (5 kW), main frequency, and active power generated by the GFMI section of the UHC-based VSIs (2.93 kW), the system frequency has decreased by 0.12 Hz. According to the amplitude droop characteristic and reactive powers supplied by the virtual GFMI section of the UHC-based VSIs, Figure 22 shows a controlled and precise reduction in the peak voltage of the output terminals relative to the rated value. To quantify the voltage drop, consider VSI#2 as an example. Given that the reference reactive power of its GFLI section is set at 1.54 kVAR and the reactive power at the PoC is 1.845 kVAR (see the red line in Figure 20), the reactive power provided by the GFMI section should be 305 VAR. Utilizing the corresponding amplitude droop coefficient (4%), the rated reactive power of the GFMI section (2.2 kVAR), and the rated peak voltage at the VSI output terminals (326.6 V), the calculated voltage drop will be precisely 1.82 V. Similar analyses confirm the controlled and exact voltage drops for other VSIs.

- **Case 2** ($2s \leq t \leq 4s$)

In Case 2, as outlined in Table 4, simultaneous sudden changes in the S_{L4} load level (25% increase) and VSIs reference powers are applied. Adjustments in the reference powers occur to alter the GFLI operational part of the three VSIs to 30%, 50%, and 60% of their rated capacity, respectively. Figures 19 and 20 show that the UHC-based VSIs demonstrate adaptability to these sudden variations and achieve fast and accurate tracking of output reference powers, along with proper load sharing among the VSIs. Figures 21 and 22 depict the controlled regulation of the frequency and voltage, highlighting the role of the UHC-based multi-VSI system in local grid support. These results validate the effectiveness of the UHC in managing dynamic load changes while ensuring system stability. Moreover, the observed dynamic response, characterized by a well-controlled and stable frequency profile following these perturbations, confirms the ability of the UHC to emulate synthetic inertia in the tested multi-VSI system. This verification indicates potential for applications in islanded power networks with high penetration of IBRs.

SCENARIO 3

Impact of Line Outage and Reconnection.

This scenario investigates the impacts of a line outage and reconnection event, as a crucial yet realistic test bed, on the performance, resilience, and adaptability of a UHC-based multi-VSI system. This study is vital for ensuring the reliability and stability of the power distribution system in the face of unforeseen events and disruptions and to emphasize its ability to recover seamlessly after line reconnection.

- **Case 3** ($4s \leq t \leq 7s$)

In this case, line 2-4, connecting VSI#2 to PoC 4, is intentionally disconnected at $t = 4s$ to emulate a line outage scenario, creating a realistic and impactful disruption in the network topology. As observed in Figures 19 and 20, accurately tracking the reference powers and proper load sharing among VSIs attest to the effectiveness of UHC in compliance with the droop characteristics. These outcomes signify the ability and robust performance of the UHC to provide reactive power support during and after a line outage. This ensures that each UHC-based VSI adapts to the changed network configuration caused by the intentional perturbations. In addition, as seen in Figures 21 and 22, the local grid parameters are also accurately controlled with stable transients, corresponding to the active and reactive powers generated by the GFMI section of each VSI.

- **Case 4** ($7s \leq t \leq 10s$)

The reconnection of line 2-4 reveals a rapid recovery, characterized by the system swiftly returning to a stable state similar to its operating conditions in Case 2 within a short time frame (see Figures 19 to 22). This expeditious restoration demonstrates the resilience and adaptability of UHC, indicating its capability in stabilizing multi-VSI islanded power systems following intentional network perturbations.

Table 5 presents a structural and performance comparison between the proposed UHC scheme and the HCC method introduced in [20]. While both approaches aim to integrate GFM and GFL functionalities within a single inverter, they feature fundamental structural differences that make them suitable for different applications.

The UHC scheme utilizes an $\alpha\beta$ frame-based control design with a PR controller, eliminating the need for a PLL. This configuration employs a parallel seamless control structure with only 5 control parameters, while the HCC method operates in the dq frame with a cascaded structure involving multiple PI controllers and internal feedback loops (described in [20]), requiring 16 control parameters in total.

A key structural distinction lies in the equivalent circuit models underlying each approach. The UHC model combines a Thevenin equivalent circuit for GFM with a current source for GFL with independent GFM/GFL control paths and direct PoC measurement inputs (Figures 8 and 9), while the HCC model employs two Thevenin equivalent circuits with a restrictive impedance ratio constraint as shown in Eqs. (3)-(4) and Figures 5 and 8 of [20].

The comprehensive simulation results presented in Section IV demonstrate that the UHC method provides effective transient response characteristics in various islanded operation scenarios, including sudden load changes, reference power variations, and local network disturbances. These simulations show millisecond-level settling times, which align with the requirements of islanded microgrids where system conditions can change rapidly. In contrast to the HCC approach, which requires more complex implementation and tuning processes due to its multiple control loops and higher parameter count, the UHC method achieves comparable or better performance with a simpler structure and fewer parameters, making it particularly suitable for isolated microgrid applications where simplicity and robustness are critical.

It is worth emphasizing that the proposed UHC scheme, developed based on the parallel operation of GFMI and GFLI

TABLE 5. Structural and performance comparison between the proposed UHC approach and the HCC method [20].

Comparison Between the Proposed UHC Approach and HCC Method [20]		
	UHC Method (Proposed)	**HCC Method [20]**
Reference Frame and Control Design	PR-controller based implementation in $\alpha\beta$ frame (PLL-free design)	PI-controllers based implementation in dq frame (requires PLL)
Control Architecture	Parallel seamless structure with independent controllers, no feedback loops	Cascaded structure with internal feedback loops between control sections (described in [20])
Control Parameters	5 parameters: 3 for PR controller & damping, 2 for GFM output filter impedance in calculations	16 parameters: 12 for PI controllers, 4 for both GFM/GFL output filter impedances in calculations
Equivalent Circuit Model	Thevenin source for GFM + current source for GFL without restrictive assumptions (Fig. 8)	Two Thevenin sources with restrictive impedance ratio constraint as noted in Eqs. (3-4) of [20]
Transient Response in Simulations	Demonstrated millisecond-level settling times in the presented islanded microgrid simulations (Figs. 11-22)	Designed for second-level responses in grid-connected applications (as reported in [20])
Target Application	Specifically designed for islanded microgrid applications	Primarily optimized for grid-connected applications

equivalent circuits, provides a flexible framework capable of accommodating various control strategies. While this study implements droop control for the GFM functionality and instantaneous power theory for the GFL functionality—both of which are well-suited to islanded microgrid applications—the UHC framework is not restricted to these specific methods. This inherent flexibility enables the integration of alternative GFM approaches, such as virtual synchronous machines [31], [32], inertia emulation techniques [33], or advanced GFL control methods focusing on enhanced current regulation and reactive power support [34], [35]. Such adaptability may offer particular value in modern islanded microgrids with high IBR penetration, where control requirements can evolve in response to local grid conditions and operational objectives.

C. LIMITATIONS AND FUTURE WORK

This study has focused specifically on the development and validation of the proposed UHC approach for islanded microgrid applications, which present unique operational challenges and control requirements compared to grid-connected systems. It is important to highlight that both the UHC and HCC methods were designed for fundamentally different primary applications (islanded and grid-connected modes, respectively). As such, a direct numerical comparison between the two methods would not be methodologically appropriate within the scope of this work.

The UHC method demonstrated effective performance across various islanded scenarios, with its PLL-free design offering notable advantages in this specific context. While PLL-free approaches generally offer benefits such as simplified implementation and avoidance of PLL-related instabilities in weak grid conditions, we acknowledge that they may encounter distinct challenges under certain operating conditions. To this end, future research will extend the validation of the UHC framework to additional scenarios, including unbalanced voltage conditions and grid frequency deviations—situations that are more frequently encountered in grid-connected environments. This will enable adaptation of the UHC approach for broader applications and allow more direct comparisons with existing control strategies under diverse and challenging conditions.

Additionally, future studies will investigate the dynamic interactions between UHC-based IBRs and synchronous machines. Gaining a deeper understanding of these interactions is expected to offer valuable insights into the performance of UHC-controlled inverters in hybrid power systems and further demonstrate their practical potential in real-world implementations.

V. CONCLUSION

The integration of IBRs in islanded microgrids presents unique challenges that require specialized control approaches. This study introduces a UHC scheme specifically designed for islanded applications, enabling a single voltage-controlled VSI to simultaneously provide GFM and GFL functionalities. While drawing inspiration from previous hybrid control concepts such as the HCC approach presented by Lima and Watanabe [20], the proposed UHC scheme presents a distinct, application-driven control structure specifically tailored for islanded microgrids, offering practical implementation advantages under such conditions. The UHC implementation features several key structural differences from previous approaches, including (1) a parallel control architecture in the $\alpha\beta$ reference frame that eliminates PLL dependency, (2) significantly reduced control parameters (three tunable parameters), (3) direct power reference tracking using instantaneous power theory without complex internal feedback loops, and (4) a simplified equivalent circuit model that avoids restrictive assumptions about system impedance values. These structural differences address the specific challenges of islanded microgrid operation, where rapid transient response and robust frequency regulation are essential. Comprehensive simulation studies conducted across diverse islanded scenarios validate the effectiveness of the proposed approach. In single-inverter configurations, the UHC-equipped VSI demonstrated precise tracking of reference powers while maintaining frequency and voltage stability during sudden load changes. When subjected to a 50% voltage drop caused by a three-phase fault, the controller successfully limited current within permissible boundaries while facilitating rapid recovery upon fault clearance. In multi-inverter configurations, the UHC scheme enabled proper load sharing between units and maintained stable operation during line outages and reconnection events. The PLL-free design of the UHC scheme provides particular advantages in islanded microgrids, where the absence of a strong frequency reference makes traditional synchronization methods less effective. The parallel, seamless, and decoupled control structure with a single PR controller in the $\alpha\beta$

reference frame simplifies implementation, while effectively fulfilling the control objectives of both the GFM and GFL functionalities without introducing cross-coupling between control objectives. These findings suggest that the UHC approach represents a valuable contribution to the field of islanded microgrid control, providing a structurally distinct alternative that balances implementation simplicity with operational effectiveness. Future research directions include investigating the interactions between UHC-controlled inverters and synchronous generators in hybrid power systems, as well as exploring the adaptability of the UHC framework to grid-connected applications, where it could be evaluated under additional challenging conditions such as unbalanced voltage faults and frequency deviations.

REFERENCES

[1] I. Lorzadeh, H. A. Abyaneh, M. Savaghebi, and J. M. Guerrero, "A hierarchical control scheme for reactive power and harmonic current sharing in islanded microgrids," in *Proc. 17th Eur. Conf. Power Electron. Appl. (EPE ECCE-Europe)*, Sep. 2015, pp. 1–10.

[2] J. Rocabert, A. Luna, F. Blaabjerg, and P. Rodríguez, "Control of power converters in AC microgrids," *IEEE Trans. Power Electron.*, vol. 27, no. 11, pp. 4734–4749, Nov. 2012.

[3] I. Lorzadeh, H. A. Abyaneh, M. Savaghebi, O. Lorzadeh, A. Bakhshai, and J. M. Guerrero, "An enhanced instantaneous circulating current control for reactive power and harmonic load sharing in islanded microgrids," *J. Power Electron.*, vol. 17, no. 6, pp. 1658–1671, 2017.

[4] D. B. Rathnayake, M. Akrami, C. Phurailatpam, S. P. Me, S. Hadavi, G. Jayasinghe, S. Zabihi, and B. Bahrani, "Grid forming inverter modeling, control, and applications," *IEEE Access*, vol. 9, pp. 114781–114807, 2021.

[5] J. Matevosyan, B. Badrzadeh, T. Prevost, E. Quitmann, D. Ramasubramanian, H. Urdal, S. Achilles, J. MacDowell, S. H. Huang, V. Vital, J. O'Sullivan, and R. Quint, "Grid-forming inverters: Are they the key for high renewable penetration?" *IEEE Power Energy Mag.*, vol. 17, no. 6, pp. 89–98, Nov. 2019.

[6] A. B. Attya, J. L. Dominguez-Garcia, and O. Anaya-Lara, "A review on frequency support provision by wind power plants: Current and future challenges," *Renew. Sustain. Energy Rev.*, vol. 81, pp. 2071–2087, Jan. 2018.

[7] W. Du, F. K. Tuffner, K. P. Schneider, R. H. Lasseter, J. Xie, Z. Chen, and B. Bhattarai, "Modeling of grid-forming and grid-following inverters for dynamic simulation of large-scale distribution systems," *IEEE Trans. Power Del.*, vol. 36, no. 4, pp. 2035–2045, Aug. 2021.

[8] L. Huang, C. Wu, D. Zhou, and F. Blaabjerg, "A double-PLLs-based impedance reshaping method for extending stability range of grid-following inverter under weak grid," *IEEE Trans. Power Electron.*, vol. 37, no. 4, pp. 4091–4104, Apr. 2022.

[9] Y. Zhou, H. Xin, D. Wu, F. Liu, Z. Li, G. Wang, H. Yuan, and P. Ju, "Small-signal stability assessment of heterogeneous grid-following converter power systems based on grid strength analysis," *IEEE Trans. Power Syst.*, vol. 38, no. 3, pp. 2566–2579, May 2023.

[10] X. Fu, J. Sun, M. Huang, Z. Tian, H. Yan, H. H. Iu, P. Hu, and X. Zha, "Large-signal stability of grid-forming and grid-following controls in voltage source converter: A comparative study," *IEEE Trans. Power Electron.*, vol. 36, no. 7, pp. 7832–7840, Jul. 2021.

[11] N. Mohammed, H. H. Alhelou, and B. Bahrani, *Grid-Forming Power Inverters: Control and Applications*. Boca Raton, FL, USA: CRC Press, 2023.

[12] K. Y. Yap, C. R. Sarimuthu, and J. M.-Y. Lim, "Virtual inertia-based inverters for mitigating frequency instability in grid-connected renewable energy system: A review," *Appli. Sci.*, vol. 9, no. 24, p. 5300, Dec. 2019.

[13] Y. Jiang, A. Bernstein, P. Vorobev, and E. Mallada, "Grid-forming frequency shaping control for low-inertia power systems," *IEEE Control Syst. Lett.*, vol. 5, no. 6, pp. 1988–1993, Dec. 2021.

[14] M. Li, H. Geng, and X. Zhang, "Hierarchical mode-dispatching control for multi-inverter power stations," *IEEE Trans. Ind. Electron.*, vol. 70, no. 10, pp. 10044–10054, Oct. 2023.

[15] M. A. Zamee, D. Han, and D.-J. Won, "Integrated grid forming-grid following inverter fractional order controller based on Monte Carlo artificial bee colony optimization," *Energy Rep.*, vol. 9, pp. 57–72, Jan. 2022.

[16] J. He and Y. W. Li, "Hybrid voltage and current control approach for DG-grid interfacing converters with LCL filters," *IEEE Trans. Ind. Electron.*, vol. 60, no. 5, pp. 1797–1809, May 2013.

[17] A. Camacho, M. Castilla, J. Miret, L. G. De Vicuña, and R. Guzman, "Positive and negative sequence control strategies to maximize the voltage support in resistive–inductive grids during grid faults," *IEEE Trans. Power Electron.*, vol. 33, no. 6, pp. 5362–5373, Jun. 2018.

[18] J. L. Rodríguez-Amenedo, S. Arnaltes-Gómez, M. Aragüés-Peñalba, and O. Gomis-Bellmunt, "Control of the parallel operation of VSC-HVDC links connected to an offshore wind farm," *IEEE Trans. Power Del.*, vol. 34, no. 1, pp. 32–41, Feb. 2019.

[19] S. Geng and I. A. Hiskens, "Unified grid-forming/following inverter control," *IEEE Open Access J. Power Energy*, vol. 9, pp. 489–500, 2022.

[20] L. A. M. Lima and E. H. Watanabe, "Hybrid control scheme for VSC presenting both grid-forming and grid-following capabilities," *IEEE Trans. Power Del.*, vol. 37, no. 6, pp. 4570–4581, Dec. 2022.

[21] Y. Lin, J. H. Eto, B. Johnson, J. Flicker, R. H. Lasseter, H. V. Pico, G. Seo, B. Pierre, and A. Ellis, "Research roadmap on grid-forming inverters," Nat. Renew. Energy Lab., Golden, CO, USA, Tech. Rep. NREL/TP-5D00-73476, 2020.

[22] J. He and Y. W. Li, "Generalized closed-loop control schemes with embedded virtual impedances for voltage source converters with LC or LCL filters," *IEEE Trans. Power Electron.*, vol. 27, no. 4, pp. 1850–1861, Apr. 2012.

[23] J. C. Vasquez, J. M. Guerrero, M. Savaghebi, J. Eloy-Garcia, and R. Teodorescu, "Modeling, analysis, and design of stationary-reference-frame droop-controlled parallel three-phase voltage source inverters," *IEEE Trans. Ind. Electron.*, vol. 60, no. 4, pp. 1271–1280, Apr. 2013.

[24] I. Lorzadeh, H. Askarian Abyaneh, M. Savaghebi, A. Bakhshai, and J. Guerrero, "Capacitor current feedback-based active resonance damping strategies for digitally-controlled inductive-capacitive-inductive-filtered grid-connected inverters," *Energies*, vol. 9, no. 8, p. 642, Aug. 2016.

[25] I. Lorzadeh, M. Savaghebi, H. A. Abyaneh, and J. M. Guerrero, "Active damping techniques for LCL-filtered inverters-based microgrids," in *Proc. IEEE 10th Int. Symp. Diag. Electr. Mach., Power Electron. Drives (SDEMPED)*, Sep. 2015, pp. 408–414.

[26] O. Lorzadeh, I. Lorzadeh, M. N. Soltani, and A. Hajizadeh, "Source-side virtual RC damper-based stabilization technique for cascaded systems in DC microgrids," *IEEE Trans. Energy Convers.*, vol. 36, no. 3, pp. 1883–1895, Sep. 2021.

[27] O. Lorzadeh, I. Lorzadeh, Mohsen. N. Soltani, and A. Hajizadeh, "A novel active stabilizer method for DC/DC power converter systems feeding constant power loads," in *Proc. IEEE 28th Int. Symp. Ind. Electron. (ISIE)*, Jun. 2019, pp. 2497–2502.

[28] S. Buso and P. Mattavelli, *Digital Control in Power Electronics*. San Rafael, CA, USA: Morgan & Claypool, 2006.

[29] H. Akagi, E. H. Watanabe, and M. Aredes, *Instantaneous Power Theory and Applications to Power Conditioning*. Hoboken, NJ, USA: Wiley, 2017.

[30] J. W. Nilsson and S. A. Riedel, *Electric Circuits*. London, U.K.: Pearson, 2019.

[31] K. Mahmoud, P. Astero, P. Peltoniemi, and M. Lehtonen, "Promising grid-forming VSC control schemes toward sustainable power systems: Comprehensive review and perspectives," *IEEE Access*, vol. 10, pp. 130024–130039, 2022.

[32] H. Zhang, W. Xiang, W. Lin, and J. Wen, "Grid forming converters in renewable energy sources dominated power grid: Control strategy, stability, application, and challenges," *J. Modern Power Syst. Clean Energy*, vol. 9, no. 6, pp. 1239–1256, Nov. 2021.

[33] R. Rosso, X. Wang, M. Liserre, X. Lu, and S. Engelken, "Grid-forming converters: Control approaches, grid-synchronization, and future trends—A review," *IEEE Open J. Ind. Appl.*, vol. 2, pp. 93–109, 2021.

[34] W. Zhou, N. Mohammed, and B. Bahrani, "Comprehensive modeling, analysis, and comparison of state-space and admittance models of PLL-based grid-following inverters considering different outer control modes," *IEEE Access*, vol. 10, pp. 30109–30146, 2022.

[35] N. Mohammed, W. Zhou, and B. Bahrani, "Comparison of PLL-based and PLL-less control strategies for grid-following inverters considering time and frequency domain analysis," *IEEE Access*, vol. 10, pp. 80518–80538, 2022.

IMAN LORZADEH (Member, IEEE) was born in Shiraz, Iran, in 1984. He received the B.S. and M.S. degrees (Hons.) in electrical engineering from Shiraz University, Shiraz, in 2006 and 2009, respectively. From 2011 to 2016, he was a Senior Research Assistant with the Department of Electrical Engineering, Amirkabir University of Technology (Tehran Polytechnic), Tehran, Iran. In 2014, he was a Visiting Researcher with the Department of Energy Technology, Aalborg University, Aalborg, Denmark. He was a Lecturer with Salman Farsi University, Iran, from 2017 to 2023. He is currently a Research Assistant with the Electrical Energy Laboratory (EELAB), Department of Electromechanical Systems and Metal Engineering, Ghent University, Ghent, Belgium. His research interests include distributed generation systems, the modeling and control of power electronics converters, power quality, power electronics-based power systems, enhancing efficiency in power electronic converters, and power electronics-based drives.

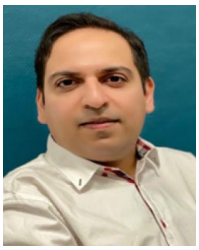

OMID LORZADEH (Student Member, IEEE) was born in Shiraz, Iran, in 1984. He received the B.S. degree in electrical and electronic engineering and the M.S. degree (Hons.) in control engineering from Shiraz University, Shiraz, Iran, in 2006 and 2011, respectively, and the Ph.D. degree in electrical engineering specializing in power electronics from the Department of Energy Technology, Aalborg University, Denmark. Throughout his career, he has embarked on various academic and industrial endeavors, showcasing his expertise and passion for advancing the field of electrical engineering. In 2020, he was a Visiting Researcher at the Center for Combined Smart Energy Systems (CoSES) in collaboration with the Technical University of Munich (TUM). Following this, he undertook a Postdoctoral Program at the University of St. Thomas, USA, from 2022 to 2023. In 2022, he transitioned to the industry, joining Volvo Group, Sweden, as a Senior Electrical Design Engineer. Since 2023, he has been a Senior Principal Electrical Engineer with the Research and Development Department (Power Electronics and Control), AmberSemi Company, San Francisco, USA. At AmberSemi, he leads the dedicated Research and Development Team focused on pioneering advancements in V2X bi-directional EV charger technology and powering AI data center projects. His research interests include the modeling and control of power converters, high-efficiency, high-density power conversion and controls, power quality, and stability issues in modern power systems.

DIMITAR V. BOZALAKOV (Senior Member, IEEE) was born in Harmanli, Bulgaria, in 1985. He received the M.S. degree in industrial electronics from TU Varna, Varna, Bulgaria, and the Ph.D. degree in electromechanical engineering from Ghent University, Ghent, Belgium, in 2011 and 2019, respectively. Since 2019, he has been a Postdoctoral Assistant with the Electrical Energy Laboratory (EELAB), Ghent University. His current research interests include electric power systems, renewable energy applications, energy storage, improving the power quality in the distribution grids, and the efficiency improvement of power electronic converters.

LUC DUPRÉ (Member, IEEE) was born in Eeklo, Belgium, in 1966. He received the degree in electrical and mechanical engineering and the Ph.D. degree in applied sciences from Ghent University, Belgium, in 1989 and 1995, respectively. In 1989, he joined the Department of Electrical Energy, Systems and Automation, Ghent University, as a Research Assistant. In 1996, he was a Postdoctoral Researcher with the Fund for Scientific Research-Flanders. In 1998, he was a Visiting Postdoctoral Fellow at the Istituto Elettrotecnico Nazionale "Galileo Ferraris," Torino, Italy, for six months. In 2002, he was an Associate Professor with the Faculty of Engineering and Architecture, Ghent University, where he has been a Full Professor, since 2006. His research interests include numerical methods for low frequency electromagnetism (in particular for electrical machines), modeling and characterization of soft magnetic materials, micromagnetism, inverse problems, and optimization in (bio)electromagnetism.

LIEVEN VANDEVELDE (Senior Member, IEEE) was born in Eeklo, Belgium, in 1968. He received the degree in electrical and mechanical engineering (main subject: electrical power engineering) and the Ph.D. degree from Ghent University, in 1992 and 1997, respectively. Since then, he has been with the Electrical Energy Laboratory (EELAB), Department of Electromechanical Systems and Metal Engineering, Ghent University. Since 2004, he has been a member of the Professorial Staff and has been coordinating the research on electric power systems at EELAB. He has conducted research in various domains of electrical power engineering, inter alia electrical machines, and (computational) electromagnetics. In this research, renewable energy and its integration into electric power systems play a prominent role.